


Soluble SARS-CoV-2 RBD and human ACE2 peptidase domain produced in *Drosophila* S2 cells show functions evoking virus–cell interface

Federico Carrión¹  | Florencia Rammauro^{1,2} | Natalia Olivero-Deibe¹ | Martín Fló^{1,2} | María Magdalena Portela^{3,4} | Analía Lima³ | Rosario Durán³ | Otto Pritsch^{1,2} | Sergio Bianchi^{5,6}

¹Laboratorio de Inmunovirología, Institut Pasteur de Montevideo, Montevideo, Uruguay

²Facultad de Medicina, Departamento de Inmunobiología, Universidad de la República, Montevideo, Uruguay

³Unidad de Bioquímica y Proteómica Analíticas, Institut Pasteur de Montevideo & Instituto de Investigaciones Biológicas Clemente Estable, Montevideo, Uruguay

⁴Facultad de Ciencias, Universidad de la República, Montevideo, Uruguay

⁵Departamento de Fisiopatología, Laboratorio de Biomarcadores Moleculares, Hospital de Clínicas, Universidad de la República, Montevideo, Uruguay

⁶Laboratorio de Genómica Funcional, Institut Pasteur de Montevideo, Montevideo, Uruguay

Correspondence

Federico Carrión, Laboratorio de Inmunovirología, Institut Pasteur de Montevideo, Montevideo, Uruguay.
Email: fcarrion@pasteur.edu.uy

Sergio Bianchi, Departamento de Fisiopatología, Laboratorio de Biomarcadores Moleculares, Hospital de Clínicas, Universidad de la República, Montevideo, Uruguay.
Email: sbianchi@pasteur.edu.uy

Funding information

Agencia Nacional de Investigación e Innovación (ANII), Grant/Award Number: FMV_3_2022_1_172395; Fondo para la Convergencia Estructural del Mercosur (FOCEM), Grant/Award Number: COF03/11

Review Editor: John Kuriyan

Abstract

The interaction between the receptor-binding domain (RBD) of the spike glycoprotein of SARS-CoV-2 and the peptidase domain of the human angiotensin-converting enzyme 2 (ACE2) allows the first specific contact at the virus–cell interface making it the main target of neutralizing antibodies. Here, we show a unique and cost-effective protocol using *Drosophila* S2 cells to produce both RBD and soluble human ACE2 peptidase domain (shACE2) as thermostable proteins, purified via Strep-tag with yields $>40 \text{ mg L}^{-1}$ in a laboratory scale. Furthermore, we demonstrate its binding with K_D values in the lower nanomolar range (independently of Strep-tag removal) and its capability to be blocked by serum antibodies in a competition ELISA with Strep-Tactin-HRP as a proof-of-concept. In addition, we assess the capacity of RBD to bind native dimeric ACE2 overexpressed in human cells and its antigen properties with specific serum antibodies. Finally, for completeness, we analyzed RBD microheterogeneity associated with glycosylation and negative charges, with negligible effect on binding either with antibodies or shACE2. Our system represents an accessible and reliable tool for designing *in-house* surrogate virus neutralization tests (sVNTs), enabling the rapid characterization of neutralizing humoral responses elicited against vaccines or infection, especially in the absence of facilities to conduct virus neutralization tests. Moreover, our biophysical and biochemical characterization of RBD and shACE2 produced in S2 cells lays the groundwork for adapting to different variants of concern (VOCs) to study humoral responses elicited against different VOCs and vaccine formulations.

KEYWORDS

ACE2, binding, *Drosophila*, microheterogeneity, neutralization, RBD, S2 cells, SARS-CoV-2, virus–cell interface

1 | INTRODUCTION

SARS-CoV-2, identified in Wuhan (China) at the end of 2019, infects humans and causes the coronavirus disease 2019 (COVID-19; Wu et al., 2020), which has led to an ongoing pandemic.

The SARS-CoV-2 virion displays on its surface a trimeric glycoprotein called spike, responsible for membrane fusion with the target cells after interacting through its receptor-binding domain (RBD) with the cellular receptor: the human angiotensin-converting enzyme 2 (hACE2; Watanabe et al., 2020; Zhao et al., 2020). The RBD is stabilized by four internal disulfides and contains a beta-stranded core that displays two N-glycosites and an extended loop spanning the receptor-binding motif (RBM; Lan et al., 2020). RBD interacts via the RBM with the peptidase domain of hACE2 (Lan et al., 2020) and is the main target of neutralizing antibodies (nABs; Goldblatt et al., 2022).

The rapid spread of SARS-CoV-2 in 2020 was followed by the fast development of effective vaccines, which were globally distributed, showing inequalities in access (Mathieu et al., 2021), concomitant with the emergence of multiple variants of concern (VOCs) with increased virulence, transmission, and immune escape (Mistry et al., 2022). In addition, different vaccine platforms have been shown to trigger a robust humoral immune response that wanes after a few months, motivating several countries to implement vaccine booster immunization that improves the response (Pascuale et al., 2022; Rammauro et al., 2022).

Vaccines distributed worldwide are based on the ancestral Wuhan variant, which was superseded by several VOCs; to date, the Omicron subvariants capable of evading antibody neutralization (Hoffmann et al., 2022; Planas et al., 2022) dominates the scene, and new “variant-based mRNA booster doses” are being evaluated (Chalkias et al., 2022) while its benefits remain on discussion (Callaway, 2022). However, as individual countries move toward approving these booster doses, the risk of repeating the history of inequity in vaccine access becomes imminent. Therefore, affordable strategies are needed to assess the multiple local contexts to minimize these effects.

In the absence of well-defined correlates of protection, measuring nABs is the best approach to determining the level of protection against SARS-CoV-2 (Goldblatt et al., 2022). The best option for determining nABs are the *plaque reduction neutralization tests* (PRNTs) and *pseudo-typed virus neutralization tests* (PVNTs), which require high-cost infrastructure and are time-consuming, further increasing the gap in testing capacity, especially in low-income countries. Despite limitations, *surrogate*

virus neutralization tests (sVNTs) have emerged as affordable and fast alternatives for studying humoral neutralizing responses (Tan et al., 2020). By its simple design based on the blockade of RBD-ACE2 binding in multi-well plates, sVNTs can be produced *in-house* and achieved in standard laboratories, giving sovereignty in vaccine decision-making, notably when lacking PRNTs or PVNTs capabilities.

As spike and hACE2 are membrane glycoproteins, eukaryotic systems remain the most suitable for recombinant production, and mammal cell systems are the most frequently used. Insect cells appear as a good alternative, overcoming some issues associated with production times, costs, and yields, as well as scalability and risk of contamination (Tripathi & Shrivastava, 2019) with baculovirus-based systems being extensively used to produce soluble SARS-CoV-2 glycoproteins (Li et al., 2020; Maffei et al., 2021; Struble et al., 2022), virus-like particles (Sullivan et al., 2022) and protein subunits vaccines (Li et al., 2022) in *Spodoptera frugiperda* and *Trichoplusia ni* cells. Baculovirus-free insect cell systems have been shown to overcome some issues in production yield in *T. ni* (Korn et al., 2020), while examples using *Drosophila melanogaster* cells are scarce (Bagdonaite et al., 2021; Creutzmacher et al., 2022).

Here, we describe a simple pipeline to produce both the RBD of SARS-CoV-2 and the soluble peptidase domain of human ACE2 (shACE2) in *Drosophila* S2 cells with minimal technical requirements and high production yields. We also characterize its behavior in solution and demonstrate its binding, revealing strengths and weaknesses of the system for studying nAB responses elicited against SARS-CoV-2.

2 | RESULTS AND DISCUSSION

2.1 | RBD and shACE2 proteins are purified from S2 culture supernatant

The recombinant protein design and their processing products are summarized in Figure 1a and described in Section 4. RBD-ST and shACE2-ST were both obtained in the culture supernatant and further purified by affinity chromatography (AC) with average yields of 40 and 60 mg L⁻¹, respectively (Supporting Information Figure S1), outperforming yields obtained with similar constructions in insect cells (Korn et al., 2020; Li et al., 2020; Maffei et al., 2021). In addition, RBD-ST and shACE2-ST were purified by size exclusion chromatography (SEC) as monomeric proteins (Figure 1b,c), with exclusion volumes corresponding to 40.2 and 87.7 kDa, respectively (Supporting Information Figure S2A,B).

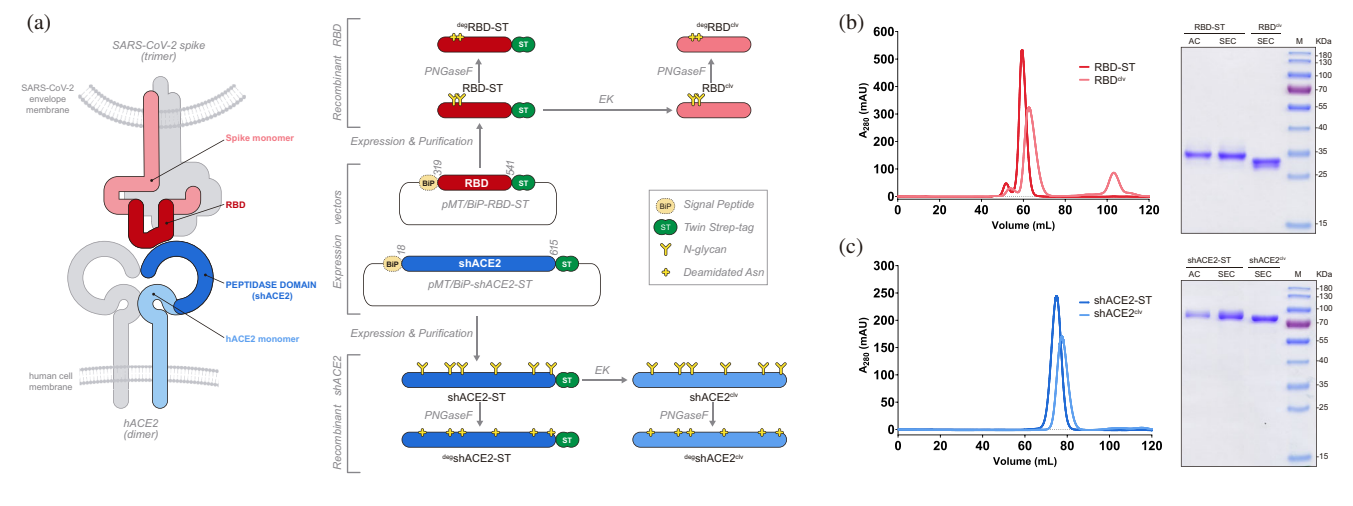


FIGURE 1 Expression and purification of RBD and shACE2 recombinant proteins. (a) Scheme showing virus–cell interface with the spike and ACE2 monomers in red and blue tones, respectively (left) and plasmids constructions with its respective processed recombinant products using the same color code (right). The names identifying each protein appear alongside each processing product (in black text) and are the same used throughout this work. (b) Preparative SEC (left) and Coomassie-stained SDS-PAGE (right) of purified RBD-ST and RBD^{clv}. (c) Preparative SEC (left) and Coomassie-stained SDS-PAGE analysis (right) of purified shACE2-ST and shACE2^{clv}. SDS-PAGE lanes are identified as AC (fractions eluted from affinity chromatography), SEC (size exclusion chromatography), and M (molecular weight marker).

2.2 | Strep-tag can be removed without compromising protein stability

As our strategy involved using the Strep-tag for multiple purposes, not only as a purification tag but also to obtain immobilized or labeled counterparts in *in vitro* binding assays, it was imperative to accomplish its removal without compromising protein stability. Consequently, upon Strep-tag removal, both RBD^{clv} and shACE2^{clv} showed an expected average size reduction of ~3 kDa (Figure 1b,c; Supporting Information Figure S2C,D), while solubility was not affected as seen by dynamic light scattering (DLS) (Supporting Information Figure S3; Supporting Information Table S1).

Both RBD-ST and RBD^{clv} showed similar thermostability by nano-differential scanning fluorimetry (nanoDSF), with broad transitions and melting temperatures (T_m) of 50.7 and 51.5°C, respectively, above those reported with a similar construction using insect cells (Li et al., 2020) (Figure 2a). Both showed reversible thermal denaturation with refolding T_m values slightly below their unfolding counterparts (50.1 and 50.4°C, respectively). RBD unfolding transition in the presence of DTT was not detected, probably due to early denaturation upon disulfide reduction (Figure 2b), which is known to have a critical role on RBD secondary structure (Grishin et al., 2022), even affecting its binding with ACE2 (Shi et al., 2022).

On the other hand, shACE2-ST and shACE2^{clv} showed irreversible thermal unfolding with narrower transitions and slightly higher T_m values (54.6 and 54.5°C, respectively), agreeing with previous reports (Glasgow et al., 2020; Figure 2c). However, as opposed to

RBD, transitions in the presence of DTT are still detected with both, showing a shift in T_m values > 10°C (Figure 2d), suggesting a less preponderant role of disulfides in shACE2 stability as previously seen in human cells expression systems (Grishin et al., 2022).

2.3 | RBD and shACE2 binding functions resembles their natural counterparts

Protein binding was measured by isothermal titration calorimetry (ITC) using two independent experimental setups (Figure 3a). Both experiments were analyzed independently, confirming 1:1 binding stoichiometry and giving very similar thermodynamic parameters with a strong enthalpic contribution reminiscent of hydrophilic molecular contacts (Lan et al., 2020), further confirming that binding is not affected upon Strep-tag removal (Supporting Information Table S2). Measured K_D values range between 17.1 and 27.0 nM, in complete agreement with those obtained in similar conditions using proteins expressed in human cells (Prévost et al., 2021).

We also evaluated binding by surface performance resonance (SPR), injecting RBD^{clv} over captured shACE2-ST. Experimental datasets obtained with variable levels of immobilized shACE2-ST gave an average $K_D = 8.29 \pm 0.69$ nM (Figure 3b; Supporting Information Table S3), consistent with proteins expressed in human (Liu et al., 2021) and insect cells (Lan et al., 2020). Additionally, we demonstrated that RBD-ST binds full-length cell-associated hACE2 in a dose-

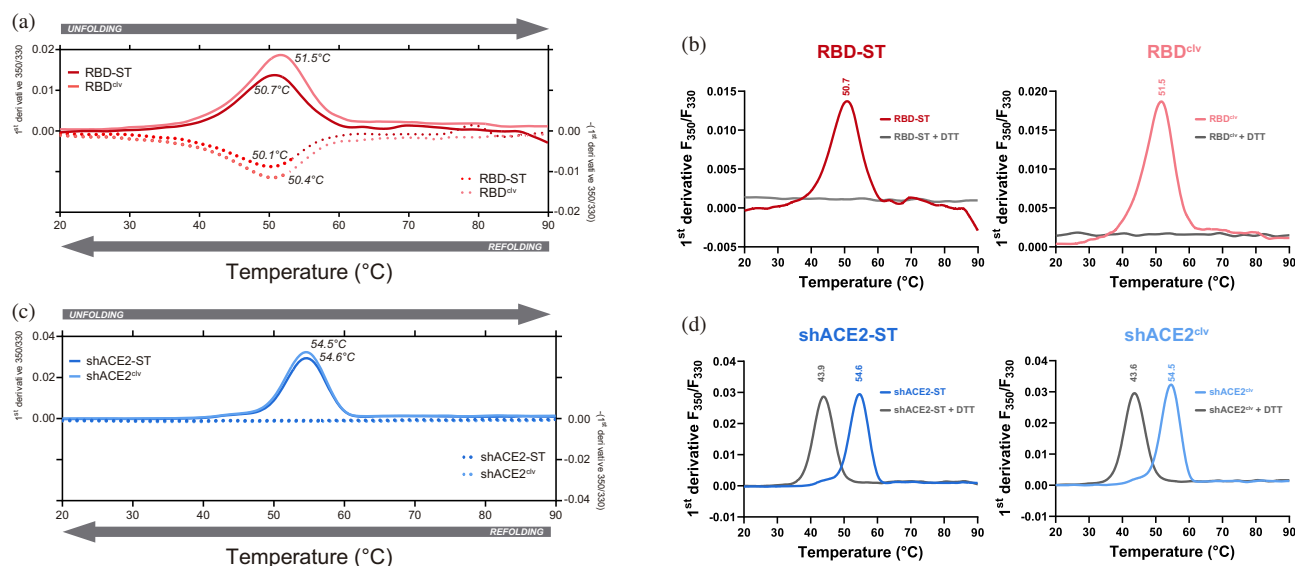


FIGURE 2 Thermostability of RBD and shACE2 recombinant proteins. (a,c) Unfolding and refolding scans obtained by nanoDSF with both RBD-ST/RBD^{clv} and shACE2-ST/shACE2^{clv}, respectively. (b,d) Unfolding scans of reduced RBD-ST/RBD^{clv} and shACE2-ST/shACE2^{clv}. Unfolding is represented with continuous lines, while refolding is shown with dotted lines using the same color code. Gray-colored traces correspond to scans done in the presence of DTT. T_m values are shown next to each transition peak.

dependent way, as seen by flow cytometry (Figure 3c), and that RBD^{clv} is specifically recognized by human sera from naturally infected individuals (Figure 3d) as seen before (Amanat et al., 2020; Rammauro et al., 2022). Finally, we demonstrate with competition ELISA that reactive serum samples can block the interaction between immobilized RBD^{clv} and soluble shACE2-ST, providing proof-of-concept for its usage in sVNTs developed *in-house* (Figure 3e).

2.4 | RBD shows microheterogeneity related with glycans and negative-charges

MALDI-TOF/TOF analysis of RBD-ST allowed us to identify three out of four total disulfide bonds (Figure 4a). The ion corresponding to the intra-peptide bridge (C₄₈₀-C₄₈₈) was detected in MS-spectrum ($m/z = x$), while the inter-peptide crosslinked cysteines (C₃₇₉-C₄₃₂ and C₃₉₁-C₅₂₅) were further corroborated by MS/MS analysis (Supporting Information Figure S4). The C₅₃₈, which forms a disulfide with a spike's domain absent in our construction, was only detected as a reduced or cysteinylated residue (Supporting Information Figure S5). Peptides containing C₃₃₆ and C₃₆₁ (which form a disulfide on the viral spike protein) were only identified after reduction/alkylation, with the peptide 329-346 containing different combinations of paucimanosidic and high mannose glycans at N₃₃₁ and N₃₄₃ (Figure 4b; Supporting Information Figure S6).

We compared RBD^{clv} and its N-deglycosylated product (degRBD^{clv}) with two-dimensional electrophoresis

(2D-SDS-PAGE), showing several spots with a variable isoelectric point (pI) below its theoretical value (pI = 8.5) (Supporting Information Figure S7,A,B). Treatment with PNGaseF evidenced a size reduction, accompanied by a relative increase in the intensity of more acidic species (probably because of asparagine deamidation) but still showing microheterogeneity due to negative charges.

We confirmed this microheterogeneity using ionic exchange chromatography (IEX) and obtaining several fractions of RBD^{clv} (hereinafter identified from *a* to *f*), which eluted differentially in a salt concentration gradient (Figure 4c). In addition, we N-deglycosylated all RBD^{clv}-IEX fractions evidencing the same electrophoretic shift in SDS-PAGE, thus suggesting that N-glycan composition is homogeneously distributed along IEX fractions and not strictly associated with charges microheterogeneity (Supporting Information Figure S7,C,D).

RBD^{clv}-IEX fractions and their deglycosylated counterparts were sequentially reduced/alkylated and subjected to nano-HPLC MS/MS analysis. As seen with MALDI-TOF/TOF, the unmodified sequence of the peptide 329-346 was not identified in any case (Supporting Information Table S4), suggesting that it is heavily modified. In parallel, we identified this peptide in all degRBD^{clv}-IEX fractions containing deamidated asparagine residues (Supporting Information Table S5). Scans corresponding to doubly-deamidated peptide 329-346 represented 91%, while deamidation in a single asparagine corresponded to 0.2% and 8.8% for N₃₃₁ and N₃₄₃, respectively (Supporting Information Table S6). These results show that N-glycan occupancy in predicted sites is

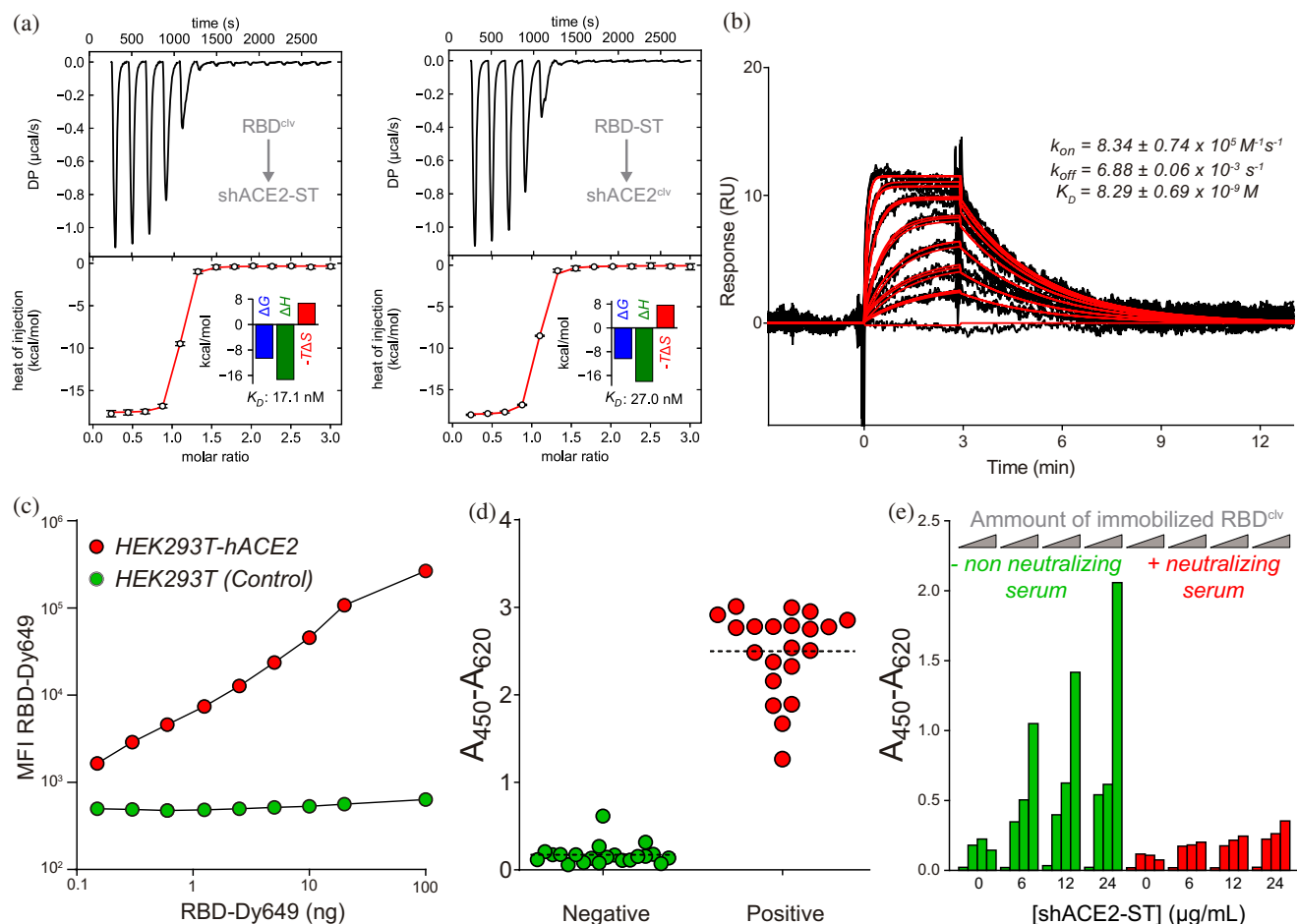


FIGURE 3 Functional analysis of RBD and shACE2 recombinant proteins. (a) ITC analysis of shACE2-ST titrated with RBD^{clv} (left panel), and shACE2^{clv} titrated with RBD-ST (right panel). Each panel comprises the corrected thermogram upon baseline subtraction (up) and a schematic representation of the titration setup (inset). The integrated heat values fitting to a hetero-association model in red (bottom) are accompanied by the thermodynamic signature and K_D values (inset). (b) Representative SPR experiment with RBD^{clv} injected over captured shACE2-ST, with superimposed sensorgrams (black) and fitting to 1:1 Langmuir interaction model (red) and the average kinetic parameters obtained in three independent experiments (Supporting Information Table S3). (c) Mean fluorescence intensity (MFI) measured by flow cytometry in cells over-expressing hACE2 (red) and control cells (green), incubated with increasing amounts of fluorescent RBD (x-axis). (d) ELISA with a set of human sera identified as negative (pre-pandemic) and positive (confirmed by PCR and a commercial anti-SARS-CoV-2 ELISA) using RBD^{clv} as antigen. (e) Competition ELISA between different concentrations of shACE2-ST (x-axis) and two serum samples: a negative non-neutralizing serum (pre-pandemic, in green) and a positive neutralizing serum (confirmed with a commercial sVNT) to bind increasing amounts of immobilized RBD^{clv} (represented with gray triangles above each group).

high, with N₃₃₁ less occupied than N₃₄₃, as seen before with RBD expressed in human and insect cells (Bagdonaite et al., 2021; Sanda et al., 2021).

Regarding mono-glycosylated peptide 329–346, we identified paucimannosidic and high-mannose glycans only on N₃₄₃ (Supporting Information Table S7), probably because of the higher occupancy mentioned above. In contrast, double glycosylated peptides were not detected, probably due to their poorer ionization efficiency and high hydrophilicity, which impedes their binding to reversed-phase columns (Kozlik et al., 2017). Based on this, we propose that such mono-glycosylated peptides constitute an infrequent fraction of glycopeptides, but one that may help us elucidate which moieties are most

abundant in RBD expressed in S2 cells without ruling out the existence of motifs with higher content in mannose.

As for O-glycosylation, Tn and Core 1-type glycans were also identified in degRBD^{clv} using nano-HPLC MS/MS. The most frequent O-glycosites were identified on threonine residues belonging to N-glycosylation sequons (T₃₃₃ and T₃₄₅), almost exclusively when the precedent N was not deamidated. This suggests that O-glycosylation only occurs at these positions in the absence of N-glycans, supporting the hypothesis that O-glycans could be masking unusually unoccupied N-glycosites on RBD expressed in S2 cells (Bagdonaite et al., 2021). In parallel, Core 1-type glycans were identified at T₃₂₃ and S₃₂₅ (with twice the frequency of Tn), as

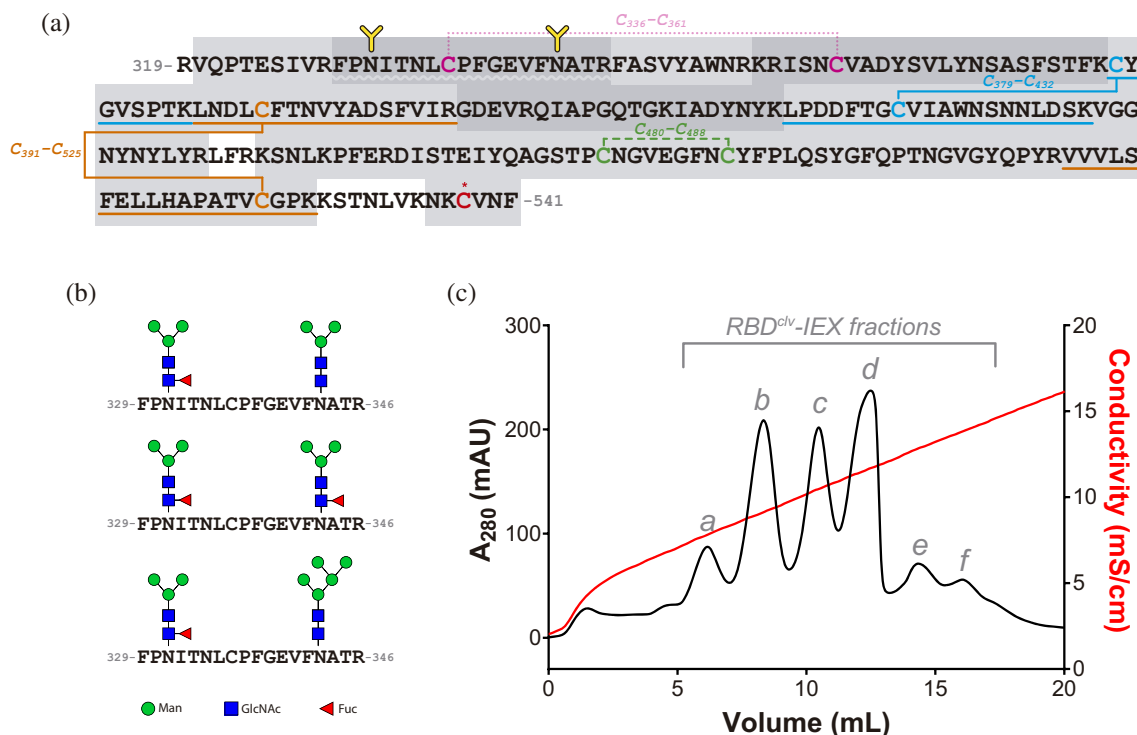


FIGURE 4 RBD micro-heterogeneity. (a) The RBD amino acid sequence is shown with gray numbers indicating the spike position of N- and C-terminal residues (cleavage and Strep-tag sequences were omitted for clarity). Disulfide bonds are shown as Cysteines (c) linked by connectors identified with a unique color code for each pair and colored labels showing the Cysteine's positions. Peptides identified by MALDI-TOF/TOF in non-reducing conditions are identified in light gray, with the identified crosslinked peptides underlined using the same color code for each disulfide and paired cysteines. Sequences marked with dark gray boxes highlight those peptides exclusively identified in reduced/alkylated RBD-ST. The disulfide represented with a dashed green line was identified as an intra-peptide bond, those identified with continuous light blue and orange connectors were identified as crosslinked peptides (Supporting Information Figure S4), and the disulfide identified with dotted lines (pale magenta) could not be directly identified by MALDI-TOF/TOF analysis. The unpaired C₅₃₈ is shown in red with an asterisk. Predicted N-glycosylation sites are shown with a yellow Y above the asparagine residues (N₃₃₁ and N₃₄₃), and the corresponding glycopeptide (between 329 and 346) is underlined with a light-gray wavy line. (b) Glycopeptide 329–346 was identified by MALDI-TOF/TOF with N-glycan modifications at N₃₃₁ and N₃₄₃. (Supporting Information Figure S6). (c) Preparative ion exchange chromatography (IEX) of RBD^{clv} showing differentially charged species named from a–f above each peak.

reported in human (Eldrid et al., 2021; Shajahan et al., 2020; Watanabe et al., 2020) and insect cells (Bagdonaite et al., 2021). Other O-glycosites were also identified with very low frequencies on RBD (Supporting Information Table S8). Our glycan characterization of RBD expressed in S2 insect cells is in full agreement with Bagdonaite et al. (2021), who used its proprietary system with different accessory sequences.

We looked for post-translational modifications (PTMs) that could explain negative charge micro-heterogeneity in RBD. Since sialylation (the most frequent source of negative charge micro-heterogeneity in glycoproteins) is rare in insect cells (Harrison & Jarvis, 2006), we excluded it from the analyses. In this regard, we found spontaneous deamidation of asparagine residues in all RBD^{clv}-IEX fractions (Supporting Information Figure S8A), with peptide #10 (spanning about half of the RBM sequence) as the most frequently deamidated peptide (Supporting Information Figure S8B). However,

as deamidation frequency was not correlated with charges, we could not solely attribute micro-heterogeneity to its occurrence. In addition, Tris adducts on deamidated asparagine (and glutamine) residues (which could be further modifying deamidated asparagine residues [Kabadi et al., 2016] and affecting its detection) remained as a very marginal fraction (0.1%–1.3%) (Supporting Information Figure S8A; Supporting Information Table S9). Asparagine deamidation to aspartate (or iso-aspartate) entails changes in overall charge (and protein backbone) and has been associated with aging in *betacoronaviruses* spike protein, with RBM described as a deamidation hotspot (Lorenzo et al., 2021). Our results suggest that deamidation in the RBM of RBD expressed in S2 cells is responsible for the presence of negative charges; however, despite our efforts, we were unable to identify a set of modifications that exclusively explain micro-heterogeneity by negative charges in RBD, and additional studies are needed to fill this gap.

2.5 | Micro-heterogeneity does not affect RBD functionality

Spike glycosylation shields its surface, keeping it away from the immune system, and even promotes conformational movements that expose RBM to hACE2 (Casalino et al., 2020; Zhao et al., 2020). However, this effect is less noticeable when the RBD is expressed as a single domain (Gstöttner et al., 2021). We used SPR to compare specific recognition by a set of sera from vaccinated individuals with RBD-ST and ^{deg}RBD-ST, not evidencing significant differences in binding (Figure 5a; Supporting Information Figure S9).

We also evaluated by SPR the effect of glycosylation on RBD-shACE2 interaction, simultaneously injecting shACE2^{clv} (or ^{deg}shACE2^{clv}) over RBD-ST and ^{deg}RBD-ST, captured in two parallel surfaces. Throughout this work, we avoided shACE2^{clv} as an analyte in SPR experiments since affinity was underestimated, probably due to non-specific interactions with the sensorchip surface. However, in this case, it allowed us to detect differences in binding accurately (if any) using virtually the same analyte injection, thus avoiding protein quantification biases. Furthermore, despite showing differences with ITC and SPR (using RBD^{clv} as an analyte), binding affinities remained invariable despite deglycosylation of captured RBD-ST (Figure 5b,c; Supporting Information Table S10), thus showing that N-glycosylation does not affect its binding, as previously shown (Sun et al., 2020).

To complete our RBD characterization, we focused on the effect of negative charge micro-heterogeneity on its binding with shACE2 and specific serum antibodies.

First, we did SPR experiments injecting RBD^{clv}-IEX fractions over captured shACE2-ST, evidencing higher affinities with respect to control experiments using pre-IEX RBD^{clv} (mainly due to higher association rate constants, k_{on} ; Figure 6a-c; Supporting Information Table S11). Since dissociation rate constant (k_{off}) fitting is independent of the analyte concentration and considering that IEX implies an extra purification step (Figure 6d), we suggest slight differences in affinities are related to protein purification/quantification. Overall, our results demonstrate that micro-heterogeneity of RBD due to negative charges has no detrimental effect on its binding with shACE2.

Finally, we immobilized RBD^{clv}-IEX fractions in multi-well ELISA plates and analyzed their antigenicity with a variable set of SARS-CoV-2 positive sera. Despite not ruling out differences in response due to protein stability upon immobilization, our results demonstrate that all RBD^{clv}-IEX fractions show antigenicity with comparable results (Figure 6e).

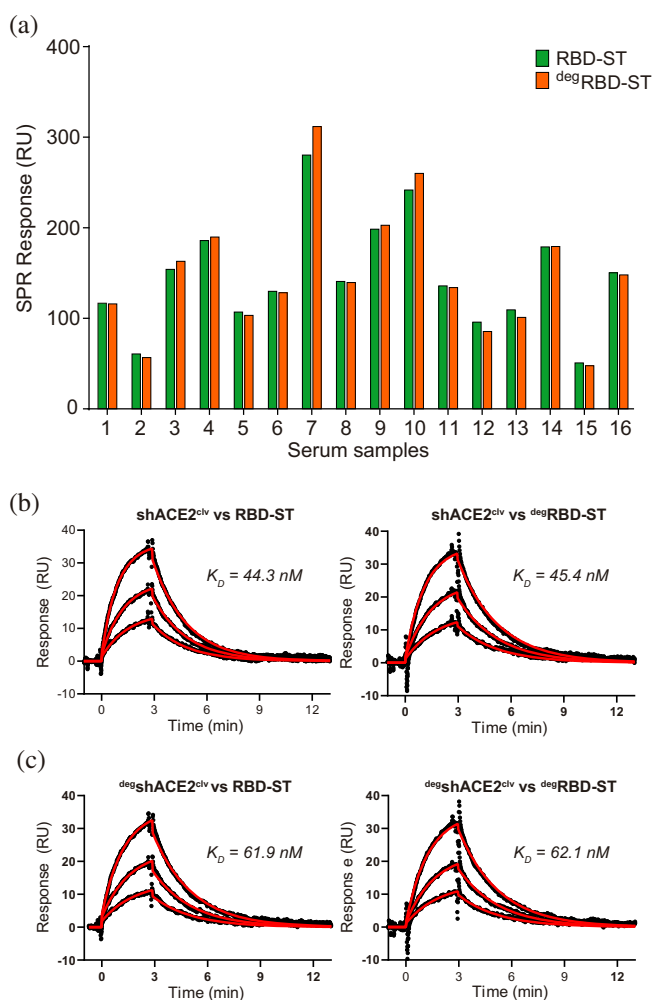


FIGURE 5 Effect of RBD N-glycosylation on binding with serum antibodies and shACE2. (a) SPR binding analysis of serum antibodies from 16 vaccinated individuals (identified with numbers 1–16) with captured RBD-ST (green bars) and ^{deg}RBD-ST (orange bars). SPR response was calculated as the average SPR signal between 1 and 1.5 min of dissociation. (b) SPR binding analysis between shACE2^{clv} injected on captured RBD-ST (left) and ^{deg}RBD-ST (right). (c) SPR binding analysis between ^{deg}shACE2^{clv} injected on captured RBD-ST (left) and ^{deg}RBD-ST (right). All SPR experiments were conducted in parallel using the same analyte injection. K_D values shown in each panel were obtained after fitting to a Langmuir 1:1 model (red traces).

3 | CONCLUSIONS

Our work is among the first to describe a cost-effective single pipeline to produce soluble versions of the SARS-CoV-2 RBD and the peptidase domain of human ACE2 using *Drosophila* S2 cells. We show they are produced with high yields, as stable and functional proteins containing or not Strep-tag. Furthermore, we found that RBD shows micro-heterogeneity due to glycosylation and variable negative charges. However, its effect on binding with ACE2 and specific antibodies is negligible,

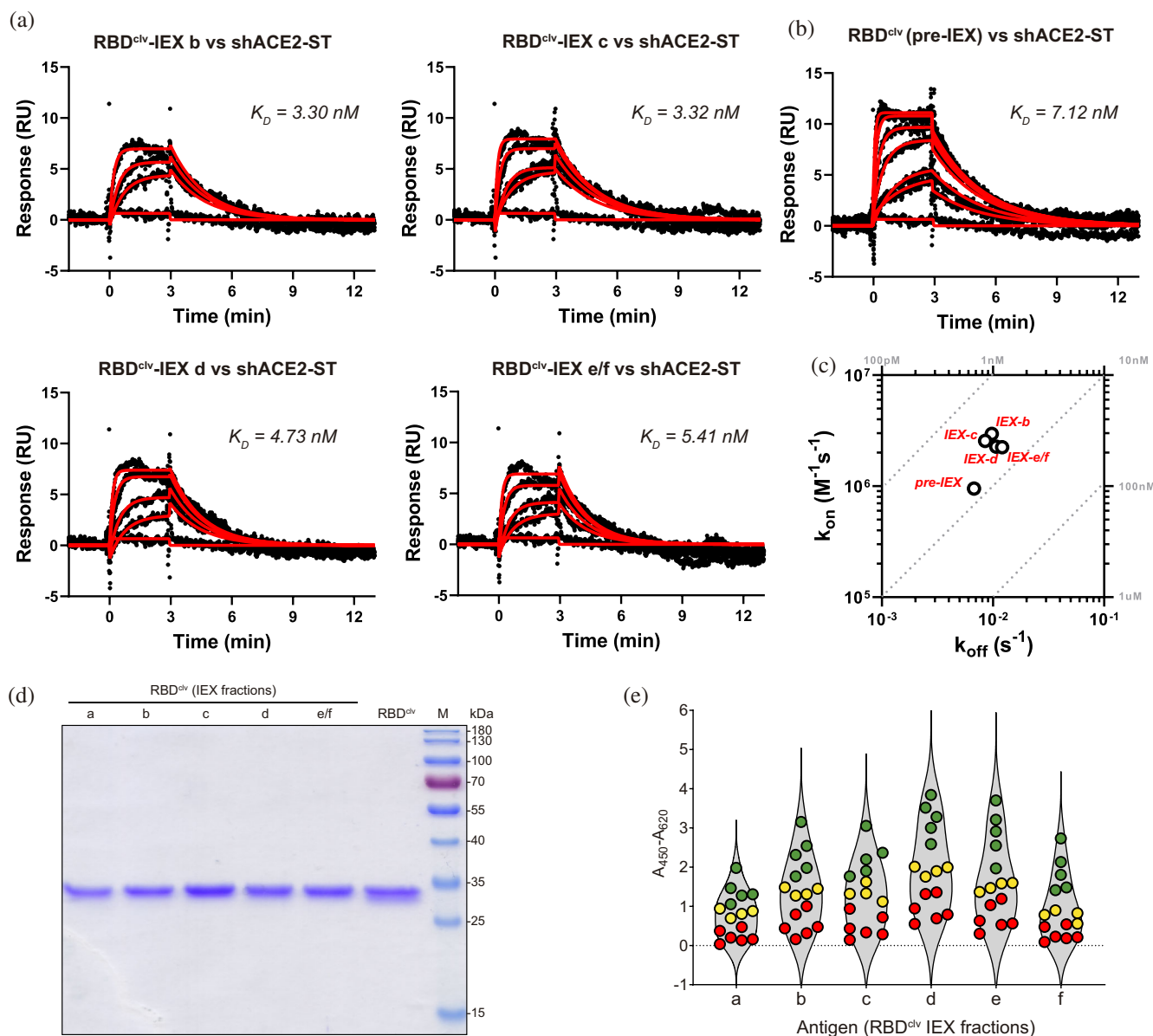


FIGURE 6 Effect of negative charges micro-heterogeneity of RBD on binding with shACE2 and serum antibodies. (a) SPR binding analysis of captured shACE2-ST with RBD^{clv}-IEX fractions and (b) control RBD^{clv} (pre-IEX). Poorly resolved e and f fractions were pooled and named e/f. All sensorgrams were fitted to a 1:1 Langmuir model (red traces) with the respective K_D values in each panel. (c) Comparison between kinetic parameters obtained by SPR in A and B, with dotted gray lines delimitating iso-affinity zones. (d) Coomassie-stained SDS-PAGE analysis of RBD^{clv}-IEX fractions after buffer exchange, protein concentration, and quantification. (e) Violin-plot of an ELISA achieved with a set of SARS-CoV-2 positive sera from infected individuals, using different RBD^{clv}-IEX fractions as antigens. For clarity, individual serum samples were arbitrarily stratified and classified with a three-color code, according to absorbance results obtained with RBD^{clv}-IEX d fraction (<1.5 are shown in red, between 1.5 and 2.5 are shown in yellow, and >2.5 are shown in green).

positioning our system as a reliable alternative to approach the virus–cell interface in vitro.

Since our work is restricted to RBD from the ancestral Wuhan variant, additional studies should be done with other VOCs in the future. Moreover, shACE2 PTMs associated with S2 cells should also be studied to characterize our system fully. Finally, as we cannot thoroughly explain the origin of charges micro-heterogeneity in RBD, we encourage researchers to assess other expression

systems and native viral proteins or immunogen formulations, looking for charges micro-heterogeneity and its effect on RBD function.

Given the results obtained in this paper, we propose RBD/shACE2 expressed in S2 cells to be used in sVNT, which can be applied in the context of limited access to BSL3, granting sovereignty in decisions making on the administration of new SARS-CoV-2 booster doses, facing each country's particular situation. Additionally, our

biophysical and biochemical characterization of proteins expressed in S2 cells strongly supports their suitability for the aforementioned applications.

4 | MATERIALS AND METHODS

4.1 | DNA constructs

DNA sequences coding for amino acids 319–541 of SARS-CoV-2 (Wuhan) spike glycoprotein (GenBank: MN908947.3) and 18–615 of hACE2 (GenBank: BAB40370.1), both fused to a C-terminal enterokinase cleavage site followed by a Twin-Strep-tag[®] (IBA) and a STOP codon, were optimized for *Drosophila* codon usage and synthesized by Genscript. Synthetic genes were cloned into a pMT/V5-His expression vector (Invitrogen) immediately after the BiP sequence as previously described (Krey et al., 2010; Figure 1a).

4.2 | Protein production

S2 stable cell lines expressing RBD-ST and shACE2-ST were obtained as described before (Rammauro et al., 2022) by co-transfection with the respective expression vector and pCoPuro selection plasmid using Efectene reagent (QIAGEN). Transfected cells were selected at 28°C in Insect Xpress medium (LONZA) added with 6 µg/mL puromycin. Stable S2 cell lines were grown in glass flasks at 28°C with 110 rpm agitation in standard orbital shaker and induced at 5×10^6 cells/mL with 5 µM CdCl₂. After 4 days of induction, cells were harvested by centrifugation at 150g for 5 min, and both proteins were purified from the culture supernatant by AC. For this, the supernatant was centrifuged at 6,000g, filtered through 0.22 µm and loaded in a 5 mL Strep-Tactin[®]XT 4Flow[®] columns (IBA), following the manufacturer's recommendations.

Strep-tag was removed by incubating overnight with Enterokinase-His (Genscript) (20 U mg⁻¹), followed by overnight dialysis in 0.1 M Tris-Cl pH 8.0, 0.15 M NaCl, incubation with Ni-Sepharose[®] (Cytiva) for 2 h and finally subjected to a second AC step in 0.1 M Tris-Cl pH 8.0, 0.15 M NaCl, 1 mM EDTA (storage buffer).

Finally, recombinant proteins were subjected to SEC in storage buffer, using Superdex 75 and 200 columns (Cytiva) for RBD-ST/RBD^{clv} and shACE2-ST/shACE2^{clv}, respectively.

4.3 | Protein analysis in solution

Purified proteins were submitted to 12% SDS-PAGE (with 0.1 M DTT when required) and further analyzed by

standard Coomassie staining or western blot using Strep-Tactin-HRP (IBA) according to the manufacturer's recommendations. In addition, two-dimensional electrophoresis was carried out as before (Lima et al., 2011) using 100 µg of RBD^{clv} and degRBD^{clv}.

The hydrodynamic radius (R_H) was analyzed by DLS in a Zetasizer Nano S (Malvern). Measurements were done in quintuplicate using quartz cuvettes at 25°C.

The thermostability of recombinant proteins was assessed by nanoDSF in a Prometheus NT.48 (Nanotemper). Unfolding and refolding T_m values were obtained upon sequential heating and cooling at 1°C/min between 20 and 90°C. When required, samples were incubated in 8000-fold excess of DTT (21–68 mM) for 1 h at 25°C.

4.4 | N-deglycosylation

N-deglycosylation was achieved under native conditions by incubating 200 µg of recombinant protein with 1000 U of PNGaseF (NEB) at 25°C overnight or under denaturant conditions at 37°C for 1 h following the recommendations of the manufacturer.

4.5 | Ion exchange chromatography

Purified proteins were buffer exchanged to 50 mM Tris pH 8.0, 10 mM NaCl using PD-10 desalting columns (Cytiva), loaded onto a Mono Q[™] 5/50 column (Cytiva) equilibrated in the same buffer for ion exchange chromatography (IEX). Then, they eluted with 50 mM Tris pH 8.0, 500 mM NaCl in a 40 CVs gradient.

4.6 | Mass spectrometry analyses

4.6.1 | Sample preparation

Sample preparation for MS was achieved with soluble proteins or bands from Coomassie-stained SDS-PAGE. When required, an initial reduction/alkylation step was conducted, as previously reported (Rivera et al., 2020). Sample preparation from SDS-PAGE bands for MALDI-TOF/TOF was done as before (Rossello et al., 2017), while for proteins in solution, tryptic peptides were obtained and desalted using C18 OMIX tips (Agilent). For MALDI-TOF/TOF, elution was performed on a plate, and for LC-MS/MS, eluates were vacuum-dried and resuspended in 0.1% formic acid as previously described (Olivero-Deibe et al., 2021).

4.6.2 | MALDI-TOF/TOF

Tryptic peptides were analyzed using a 4800 MALDI-TOF/TOF (Abi Sciex). Spectra were acquired in reflector mode, and MS/MS analysis was performed for selected ions. Proteins were identified by database searching NCBI (20160821) using MASCOT search engine (Matrix Science <http://www.matrixscience.com>) and the following parameters: monoisotopic mass tolerance, 0.03 Da; fragment mass tolerance, 0.5 Da; methionine oxidation as variable modifications, and cysteine carbamidomethylation as fixed modification (when corresponds). In addition, unassigned intense signals were fragmented for manual interpretation of N-glycosylation.

4.6.3 | LC-MS/MS analysis

Tryptic peptides were subjected to LC-MS/MS as before (Olivero-Deibe et al., 2021) using a gradient from 0% to 35% of mobile phase B over 90 min, and mass analysis was performed in a data-dependent mode using a top 12 method (Rivera et al., 2020). Database searches were performed using a *D. melanogaster* target-decoy database containing RBD sequence from Uniprot (June 2020) using PatternLab V (Santos et al., 2022). Searching parameters are listed in Supporting Information tables, and peptide spectrum matches were filtered to reach FDR $\leq 1\%$ at the protein level.

4.6.4 | Isothermal titration calorimetry

ITC was done on a VP-ITC (Malvern Panalytical) by titrating 10 μM shACE2-ST or shACE2^{clv} with 150 μM RBD^{clv} or RBD-ST, respectively, in storage buffer at 25°C. Data analysis and fitting to a hetero-association model were done as before (Medeiros et al., 2020).

4.6.5 | Surface plasmon resonance

SPR experiments were done at 25°C and flowrate of 10 $\mu\text{L}/\text{min}$ using a Biacore 3000, with 0.01 M HEPES pH 7.4, 0.15 M NaCl, 3 mM EDTA, 0.005% (v/v) P20 as running buffer, and CM5 sensorchips (Cytiva) previously coated with Twin-Strep-tag[®] Capture Kit (IBA), according to recommendations of the manufacturer. All sensorgrams were double-referenced and analyzed with BIAevaluation software v4.1.

Binding analyses were done by capturing shACE2-ST (at densities between 44 and 88 RUs) and injecting RBD^{clv} in triplicates at 2-fold increasing concentrations from 3 to 192 nM. In addition, the glycosylation effect on

binding was assayed by capturing RBD-ST (or ^{deg}RBD-ST) at densities of 35 and 25 RUs, respectively, and injecting shACE2^{clv} (or ^{deg}shACE2^{clv}) at 2-fold increasing concentrations from 12.5 to 50 nM.

The effect of RBD deglycosylation on binding with serum antibodies was assessed by SPR analysis as before (Rammauro et al., 2022), capturing RBD-ST and ^{deg}RBD-ST at final densities of 46 and 52 RUs in two parallel surfaces and injecting 1:50 dilutions of sera from individuals who received a three doses heterologous vaccination scheme (two doses of CoronaVac + booster with BNT162b).

The effect of RBD negative charges microheterogeneity on binding with shACE2-ST was evaluated by capturing ligand densities of 50 RUs and injecting RBD^{clv}-IEX fractions (b, c, d, and e/f) at concentrations of 5, 10, 25, and 50 nM. Control experiments with pre-IEX RBD^{clv} were done identically with additional 100 and 200 nM injections.

4.6.6 | Cell-surface binding assay

Assays were done as previously described (Pallesen et al., 2017) with adaptations. Briefly, 1×10^5 HEK293T and HEK293T-hACE2 (NR-52511, BEI Resources, NIAID, NIH) cells were incubated on ice for 1 h with different amounts of RBD-ST (0.15–100 ng) and subsequently stained with 1:400 Strep-Tactin-Dye 649 (IBA). Cells were immediately acquired using an Accuri C6 (BD Biosciences) and analyzed with FlowJo software (Tree Star Inc.). Unstained cells were used as a control of the fluorescence background.

4.6.7 | ELISA

ELISA was done as previously described (Rammauro et al., 2022) using plates coated with 200 ng of RBD^{clv} or RBD^{clv}-IEX fractions and incubated with 1:100 dilutions of negative (pre-pandemic), positive (SARS-CoV-2 infection confirmed by PCR), or vaccinated (two doses of CoronaVac + booster with BNT162b) human sera. Competition ELISA was done with plates coated with variable amounts of RBD^{clv} (0.0, 0.5, 1.0, and 2.0 micrograms per well) and incubated for 1 h at RT with a pre-mix of variable concentrations of shACE2-ST (0, 6, 12, and 24 $\mu\text{g}/\text{mL}$) and human sera diluted 1:20 in PBS. After washing with PBS + 0.2% Tween 20, plates were incubated with Strep-Tactin-HRP (IBA) diluted 1:1.000 and developed with TMB liquid substrate (Sigma).

This study was approved by the ethical institutional review board (MSP_956220-CEI_001-2021). Informed consent was obtained from all participants.

ACKNOWLEDGMENTS

The authors gratefully acknowledge the Cell Biology Unit at the Institut Pasteur de Montevideo for their support and assistance in the present work. The following reagents were obtained through BEI Resources, NIAID, and NIH: Human Embryonic Kidney Cells (HEK-293T) Expressing Human Angiotensin-Converting Enzyme 2, HEK-293 T-hACE2 Cell Line, NR-52511.

FUNDING INFORMATION

This work was supported by Fondo para la Convergencia Estructural del Mercosur (FOCEM, grant number COF03/11) and Agencia Nacional de Investigación e Innovación (ANII, grant number FMV_3_2022_1_172395).

ORCID

Federico Carrión  <https://orcid.org/0000-0003-4092-2168>

REFERENCES

- Amanat F, Stadlbauer D, Strohmeier S, Nguyen THO, Chromikova V, McMahon M, et al. A serological assay to detect SARS-CoV-2 seroconversion in humans. *Nat Med*. 2020;26:1033–6.
- Bagdonaite I, Thompson AJ, Wang X, Søgaard M, Fougeroux C, Frank M, et al. Site-specific O-glycosylation analysis of SARS-CoV-2 spike protein produced in insect and human cells. *Viruses*. 2021;13:551.
- Callaway E. New omicron-specific vaccines offer similar protection to existing boosters. *Nature*. 2022;609:232–3.
- Casalino L, Gaieb Z, Goldsmith JA, Hjorth CK, Dommer AC, Harbison AM, et al. Beyond shielding: the roles of Glycans in the SARS-CoV-2 spike protein. *ACS Cent Sci*. 2020;6:1722–34.
- Chalkias S, Harper C, Vrbicky K, Walsh SR, Essink B, Brosz A, et al. A bivalent omicron-containing booster vaccine against Covid-19. *N Engl J Med*. 2022;387:1279–91. Available from: <http://www.nejm.org/doi/10.1056/NEJMoa2208343>
- Creutzmacher R, Maass T, Veselkova B, Ssebyatika G, Krey T, Empting M, et al. NMR experiments provide insights into ligand-binding to the SARS-CoV-2 spike protein receptor-binding domain. *J Am Chem Soc*. 2022;144:13060–5. Available from: <http://n2t.net/addgene:154754>
- Eldrid CFS, Allen JD, Newby ML, Crispin M. Suppression of O-linked glycosylation of the SARS-CoV-2 spike by quaternary structural restraints. *Anal Chem*. 2021;93:14392–400.
- Glasgow A, Glasgow J, Limonta D, Solomon P, Lui I, Zhang Y, et al. Engineered ACE2 receptor traps potentially neutralize SARS-CoV-2. *Proc Natl Acad Sci U S A*. 2020;117:28046–55.
- Goldblatt D, Alter G, Crotty S, Plotkin SA. Correlates of protection against SARS-CoV-2 infection and COVID-19 disease. *Immunol Rev*. 2022;310:6–26.
- Grishin AM, Dolgova NV, Landreth S, Fiset O, Pickering IJ, George GN, et al. Disulfide bonds play a critical role in the structure and function of the receptor-binding domain of the SARS-CoV-2 spike antigen. *J Mol Biol*. 2022;434:167357.
- Gstöttner C, Zhang T, Resemann A, Ruben S, Pengelley S, Suckau D, et al. Structural and functional characterization of SARS-CoV-2 RBD domains produced in mammalian cells. *Anal Chem*. 2021;93:6839–47.
- Harrison RL, Jarvis DL. Protein N-glycosylation in the baculovirus–insect cell expression system and engineering of insect cells to produce “Mammalianized” recombinant glycoproteins. *Adv Virus Res*. 2006;68:159–91. Available from: <https://linkinghub.elsevier.com/retrieve/pii/S0065352706680056>
- Hoffmann M, Krüger N, Schulz S, Cossmann A, Rocha C, Kempf A, et al. The omicron variant is highly resistant against antibody-mediated neutralization: implications for control of the COVID-19 pandemic. *Cell*. 2022;185:447–456.e11. Available from: <https://linkinghub.elsevier.com/retrieve/pii/S0092867421014951>
- Kabadi PG, Sankaran K, Palanivelu DV, Adhikary L, Khedkar A, Chatterjee a mass spectrometry based mechanistic insights into formation of Tris conjugates: implications on protein biopharmaceutics. *J Am Soc Mass Spectrom*. 2016;27:1677–85.
- Korn J, Schäckermann D, Kirmann T, Bertoglio F, Steinke S, Heisig J, et al. Baculovirus-free insect cell expression system for high yield antibody and antigen production. *Sci Rep*. 2020;10:21393.
- Kozlik P, Goldman R, Sanda M. Study of structure-dependent chromatographic behavior of glycopeptides using reversed phase nanoLC. *Electrophoresis*. 2017;38:2193–9. Available from: <https://onlinelibrary.wiley.com/doi/full/10.1002/elps.201600547>
- Krey T, D'Alayer J, Kikuti CM, Saulnier A, Damier-Piolle L, Petitpas I, et al. The disulfide bonds in glycoprotein E2 of hepatitis C virus reveal the tertiary organization of the molecule. *PLoS Pathog*. 2010;6:e1000762 Available from: <https://dx.plos.org/10.1371/journal.ppat.1000762>
- Lan J, Ge J, Yu J, Shan S, Zhou H, Fan S, et al. Structure of the SARS-CoV-2 spike receptor-binding domain bound to the ACE2 receptor. *Nature*. 2020;581:215–20.
- Li L, Honda-Okubo Y, Baldwin J, Bowen R, Bielefeldt-Ohmann H, Petrovsky N. Covax-19/Spikogen[®] vaccine based on recombinant spike protein extracellular domain with Advax-CpG55.2 adjuvant provides single dose protection against SARS-CoV-2 infection in hamsters. *Vaccine*. 2022;40:3182–92.
- Li T, Zheng Q, Yu H, Wu D, Xue W, Xiong H, et al. SARS-CoV-2 spike produced in insect cells elicits high neutralization titres in non-human primates. *Emerg Microbes Infect*. 2020;9:2076–90.
- Lima A, Durán R, Schujman GE, Marchissio MJ, Portela MM, Obal G, et al. Serine/threonine protein kinase PrkA of the human pathogen listeria monocytogenes: biochemical characterization and identification of interacting partners through proteomic approaches. *J Proteomics*. 2011;74:1720–34.
- Liu H, Zhang Q, Wei P, Chen Z, Aviszus K, Yang J, et al. The basis of a more contagious 501Y.V1 variant of SARS-CoV-2. *Cell Res*. 2021;31:720–2.
- Lorenzo R, Defelipe LA, Aliperti L, Niebling S, Custódio TF, Löw C, et al. Deamidation drives molecular aging of the SARS-CoV-2 spike protein receptor-binding motif. *J Biol Chem*. 2021;279:101175 Available from: <http://www.jbc.org/article/S0021925821009777/fulltext>
- Maffei M, Montemiglio LC, Vitagliano G, Fedele L, Sellathurai S, Bucci F, et al. The nuts and bolts of SARS-CoV-2 spike receptor-binding domain heterologous expression. *Biomolecules*. 2021;11:1812.
- Mathieu E, Ritchie H, Ortiz-Ospina E, Roser M, Hasell J, Appel C, et al. A global database of COVID-19 vaccinations. *Nat Hum*

- Behav. 2021;5:947–53. Available from: <https://www.nature.com/articles/s41562-021-01122-8>
- Medeiros A, Benítez D, Korn RS, Ferreira VC, Barrera E, Carrión F, et al. Mechanistic and biological characterisation of novel N 5-substituted paullones targeting the biosynthesis of trypanothione in *Leishmania*. *J Enzyme Inhib Med Chem*. 2020;35:1345–58. Available from: <https://www.tandfonline.com/action/journalInformation?journalCode=ienz20>
- Mistry P, Barmania F, Mellet J, Peta K, Strydom A, Viljoen IM, et al. SARS-CoV-2 variants, vaccines, and host immunity. *Front Immunol*. 2022;12:1–21. Available from: <https://www.frontiersin.org/articles/10.3389/fimmu.2021.809244/full>
- Olivero-Deibe N, Tomé-Poderti L, Carrión F, Bianchi S, Fló M, Prieto D, et al. Expression, purification, and characterization of bovine leukemia virus-like particles produced in *Drosophila* S2 cells. *Frontiers in Virology*. 2021;1:756559.
- Pallesen J, Wang N, Corbett KS, Wrapp D, Kirchdoerfer RN, Turner HL, et al. Immunogenicity and structures of a rationally designed prefusion MERS-CoV spike antigen. *Proc Natl Acad Sci U S A*. 2017;114:E7348–57. Available from: <https://www.pnas.org/doi/abs/10.1073/pnas.1707304114>
- Pascuale CA, Varese A, Ojeda DS, Pasinovich ME, Lopez L, Rossi AH, et al. Immunogenicity and reactogenicity of heterologous immunization against SARS CoV-2 using sputnik V, ChAdOx1-S, BBIBP-CorV, Ad5-nCoV, and mRNA-1273. *Cell Rep Med*. 2022;3:100706 Available from: <https://linkinghub.elsevier.com/retrieve/pii/S2666379122002488>
- Planas D, Saunders N, Maes P, Guivel-Benhassine F, Planchais C, Buchrieser J, et al. Considerable escape of SARS-CoV-2 omicron to antibody neutralization. *Nature*. 2022;602:671–5. Available from: <https://www.nature.com/articles/s41586-021-04389-z>
- Prévost J, Richard J, Gasser R, Ding S, Fage C, Anand SP, et al. Impact of temperature on the affinity of SARS-CoV-2 spike glycoprotein for host ACE2. *J Biol Chem*. 2021;297:101151 Available from: <https://linkinghub.elsevier.com/retrieve/pii/S0021925821009522>
- Rammauro F, Carrión F, Olivero-Deibe N, Fló M, Ferreira A, Pritsch O, et al. Humoral immune response characterization of heterologous prime-boost vaccination with CoronaVac and BNT162b2. *Vaccine*. 2022;40:5189–96. Available from: <https://linkinghub.elsevier.com/retrieve/pii/S0264410X22009112>
- Rivera B, Leyva A, Portela MM, Moratorio G, Moreno P, Durán R, et al. Quantitative proteomic dataset from oro- and nasopharyngeal swabs used for COVID-19 diagnosis: detection of viral proteins and host's biological processes altered by the infection. *Data Brief*. 2020;32:106121.
- Rossello J, Lima A, Gil M, Duarte JR, Correa A, Carvalho PC, et al. The EAL-domain protein FcsR regulates flagella, chemotaxis and type III secretion system in *Pseudomonas aeruginosa* by a phosphodiesterase independent mechanism. *Sci Rep*. 2017;7:1–4.
- Sanda M, Morrison L, Goldman R. N- and O-glycosylation of the SARS-CoV-2 spike protein. *Anal Chem*. 2021;93:2003–9. Available from: <https://pubs.acs.org/doi/10.1021/acs.analchem.0c03173>
- Santos MDM, Lima DB, Fischer JSG, Clasen MA, Kurt LU, Camillo-Andrade AC, et al. Simple, efficient and thorough shotgun proteomic analysis with PatternLab V. *Nature Protocols*. 2022;17:1553–78. Available from: <https://www.nature.com/articles/s41596-022-00690-x>
- Shajahan A, Supekar NT, Gleinich AS, Azadi P. Deducing the N- and O-glycosylation profile of the spike protein of novel coronavirus SARS-CoV-2. *Glycobiology*. 2020;30:981–8.
- Shi Y, Zeida A, Edwards CE, Mallory ML, Sastre S, Machado MR, et al. Thiol-based chemical probes exhibit antiviral activity against SARS-CoV-2 via allosteric disulfide disruption in the spike glycoprotein. *Proc Natl Acad Sci U S A*. 2022;119:e2120419119 Available from: <https://pnas.org/doi/full/10.1073/pnas.2120419119>
- Struble LR, Smith AL, Lutz WE, Grubbs G, Sagar S, Bayles KW, et al. Insect cell expression and purification of recombinant SARS-COV-2 spike proteins that demonstrate ACE2 binding. *Protein Sci*. 2022;31:e4300.
- Sullivan E, Sung PY, Wu W, Berry N, Kempster S, Ferguson D, et al. SARS-CoV-2 virus-like particles produced by a single recombinant Baculovirus generate anti-S antibody and protect against variant challenge. *Viruses*. 2022;14:914.
- Sun Z, Ren K, Zhang X, Chen J, Jiang Z, Jiang J, et al. Mass spectrometry analysis of newly emerging coronavirus HCoV-19 spike protein and human ACE2 reveals camouflaging Glycans and unique post-translational modifications. *Engineering*. 2020;7:1441–51. Available from: <https://pubmed.ncbi.nlm.nih.gov/32904601/>
- Tan CW, Chia WN, Qin X, Liu P, Chen MI-C, Tiu C, et al. A SARS-CoV-2 surrogate virus neutralization test based on antibody-mediated blockage of ACE2-spike protein-protein interaction. *Nat Biotechnol*. 2020;38:1073–8.
- Tripathi NK, Shrivastava A. Recent developments in bioprocessing of recombinant proteins: expression hosts and process development. *Front Bioeng Biotechnol*. 2019;7:420.
- Watanabe Y, Allen JD, Wrapp D, McLellan JS, Crispin M. Site-specific glycan analysis of the SARS-CoV-2 spike. *Science*. 2020;369:330–3.
- Wu F, Zhao S, Yu B, Chen Y-M, Wang W, Song Z-G, et al. A new coronavirus associated with human respiratory disease in China. *Nature*. 2020;579:265–9.
- Zhao P, Praissman JL, Grant OC, Cai Y, Xiao T, Rosenbalm KE, et al. Virus-receptor interactions of glycosylated SARS-CoV-2 spike and human ACE2 receptor. *Cell Host Microbe*. 2020;28:586–601.e6. Available from: <https://linkinghub.elsevier.com/retrieve/pii/S1931312820304571>

SUPPORTING INFORMATION

Additional supporting information can be found online in the Supporting Information section at the end of this article.

How to cite this article: Carrión F, Rammauro F, Olivero-Deibe N, Fló M, Portela MM, Lima A, et al. Soluble SARS-CoV-2 RBD and human ACE2 peptidase domain produced in *Drosophila* S2 cells show functions evoking virus–cell interface. *Protein Science*. 2023;32(8):e4721. <https://doi.org/10.1002/pro.4721>